Nanoscale

PAPER

View Article Online
View Journal | View Issue

Cite this: *Nanoscale*, 2021, **13**, 7678

Target-switchable DNA hydrogels coupled with a $Bi_2Sn_2O_7/Bi_2S_3$ heterojunction based on *in situ* anion exchange for the "signal-on" photoelectrochemical detection of DNA†

Hongkun Li, Qianqian Cai, Xiaoshi Yan and Guifen Jie *

In this paper, a novel photoelectrochemical (PEC) "signal-on" biosensor based on a $Bi_2Sn_2O_7/Bi_2S_3$ heterojunctioncoupled with target-switchable DNA hydrogels is reported for the ultrasensitive detection of P53 gene DNA. For the first time, sulfide ions are discovered to display an excellent PEC sensitization effect on $Bi_2Sn_2O_7$ material by forming the $Bi_2Sn_2O_7/Bi_2S_3$ heterojunction. The sensitization amplitude increased by 63 times, and the photocurrent polarity switched from cathodic to anodic. When the target DNA-induced-cycling amplification process produced a mass of product chains (PD), PD was introduced into the target-switchable DNA hydrogels to quantitatively release sulfide ions, which were further introduced to the $Bi_2Sn_2O_7$-modified PEC platform and resulted in an enormous enhancement of the PEC signal due to the significant sensitization effect of sulfide ions on $Bi_2Sn_2O_7$ *via* an anion-exchange reaction. The corresponding PEC signal change of the $Bi_2Sn_2O_7/Bi_2S_3$ platform was used for the detection of target DNA. This biosensing strategy opens up a novel sulfide ion-sensitized PEC platform and exhibits excellent analytical performance with a wide linear range (100 fM–10 nM), which has broad application prospects in bioanalysis and clinical diagnosis.

Received 27th January 2021,
Accepted 30th March 2021

DOI: 10.1039/d1nr00573a

rsc.li/nanoscale

Introduction

Photoelectrochemical (PEC) biosensors, which have been widely used in the sensitive detection of various biomarkers are a new detection technology developed based on photoelectrochemistry.[1–3] The performance of biosensors depends on the use of semiconductor photoactive materials.[4–7] However, the recombination speed of photogenerated carriers in a single semiconductor is fast and the absorption efficiency of visible light is low, which restricts their practical application.[8] The construction of heterojunctions has become a common method for suppressing the recombination of photogenerated carriers.[9] By combining two kinds of semiconductors with unequal band structures, it can promote the effective transfer of photogenerated carriers, and also enhance the absorption intensity of visible light and the efficiency of the photoelectric conversion, thus further reducing the detection limit of the biosensor and expanding its application range.[10,11]

Hydrogels have attracted a lot of attention as potential sensing materials for the preparation of biosensors due to their ideal porous structure, swelling properties, and mechanical strength.[12,13] As such, the hydrogel technology has been widely employed in the domain of fluorescence,[14,15] colorimetry,[16] and electrochemistry,[17] among others. However, in this work, DNA hydrogels were applied to photoelectrochemistry for the first time. Acrylamide-modified-DNA strands were combined with polyacrylamide to construct a hybrid hydrogel, which not only reduces the amount of DNA, but also improves the stability of hydrogels.[18] Furthermore, the hydrogel was flexibly designed as a DNA-switchable structure to "open" or "close" in the presence or absence of the target.[19]

Nucleic acid analysis has become more and more important in tumor diagnosis, food hygiene and other related fields over the last few years.[20] P53, in particular, is one of the most critical tumor suppressor genes because of its dysfunction in majority human cancers.[21] This gene encodes a tumor suppressor protein containing transcriptional activation, DNA binding and oligomerization domains.[22–24] As such, the model DNA (fragment sequence of P53 gene) as the target for the assay has important clinical significance.

The cation exchange reaction was developed based on the theory of hard–soft acids and bases.[25–27] For example, soft Lewis acid ions (Cu^+, Ag^+) can be easily replaced by hard ones

Key Laboratory of Optic-electric Sensing and Analytical Chemistry for Life Science, MOE; Shandong Key Laboratory of Biochemical Analysis; Qingdao University of Science and Technology, Qingdao 266042, PR China. E-mail: guifenjie@126.com

†Electronic supplementary information (ESI) available: Experimental section, and supporting figures and tables. See DOI: 10.1039/d1nr00573a

(Ga^{3+}, Zn^{2+}) and Mn^{2+}.[28] However, the anion exchange reactions are less common because anions are usually larger and slower than cations, and therefore require more stringent conditions.[29] This paper reports an *in situ* anion exchange reaction that can be carried out at room temperature. The $Bi_2Sn_2O_7$/Bi_2S_3 heterojunction was formed by the *in situ* ion exchange between S^{2-} and $Bi_2Sn_2O_7$ photoactive material.

Herein, we report an innovative PEC sensor based on target-responsive DNA hydrogels and S^{2-}-sensitizing-$Bi_2Sn_2O_7$ by the anion-exchange reaction. The construction principle of the PEC biosensor is shown in Scheme 1. Capture DNA (CP-NH_2) was firstly connected to the carboxyl-modified silica microspheres (SiO_2–COOH) *via* covalent bonds, then CP was hybridized with product chains (PD) to obtain SiO_2-CP-PD. When the target DNA was present, it hybridized with CP on the SiO_2 microspheres to expose the recessed 3′ end of the CP chain. Exo III preferred to act on the substrate with the flat or recessed 3′ end of the DNA double chain, so the present Exo III catalyzed the stepwise removal of mononucleotides from the 3′ hydroxyl terminus of the CP chain to release the target and PD. The target was reused for the next cycle and Exo III continued to catalyze the hydrolysis of the CP chain, thus releasing a large amount of product chain PD. Meanwhile, the target-switchable DNA hydrogels were prepared. In the presence of initiator APS and accelerator TEMED, the acrydite-modified DNA strand P1 and P2 formed the polyacrylamide–DNA polymer P-A and P-B, respectively. Then P-A, P-B, linker DNA (LD) and sodium sulfide (Na_2S) were mixed to prepare DNA hydrogel for encapsulating Na_2S. After PD was added to the DNA hydrogel and induced its collapse due to the binding of PD with LD, the sulfion was quantitatively released and introduced into the $Bi_2Sn_2O_7$/electrode to obtain the heterojunction $Bi_2Sn_2O_7$/Bi_2S_3, leading to an enhanced photocurrent for target detection.

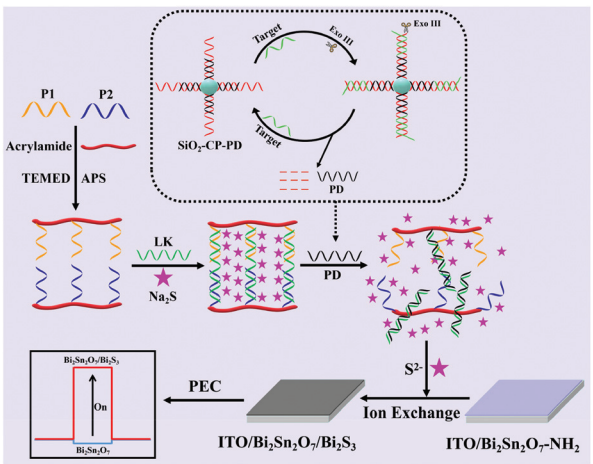

Scheme 1 Schematic representation for the PEC biosensor based on the $Bi_2Sn_2O_7$/Bi_2S_3 heterojunction coupled with target-switchable DNA hydrogels for ultrasensitive DNA detection.

Experimental section

Synthesis of $Bi_2Sn_2O_7$

$Bi_2Sn_2O_7$ was prepared by a hydrothermal method with some modifications.[30] First, 1.0 g $SnCl_4{\cdot}5H_2O$ was dissolved in 22 mL of deionized water and stirred vigorously for 15 min. Secondly, the solution pH was adjusted to 6 with 4 M sodium hydroxide, and a large amount of white sediment was generated. After centrifugation, the white precipitate was mixed with 2.2 g $Bi(NO_3)_3{\cdot}5H_2O$ and dispersed again in 45 mL of deionized water. Then, the resulting suspension pH was adjusted to 12 with sodium hydroxide, and the solution was subsequently transferred to a Teflon-lined autoclave and held at 180 °C for 24 h. The resulting product was washed three times with deionized water. $Bi_2Sn_2O_7$ was subsequently dried at 80 °C.

Fabrication of the biosensing system for detecting targets with DNA hydrogel

$Bi_2Sn_2O_7$ powder (0.5 mg) was ultrasonically dispersed in 1.0 mL of 0.5 wt% chitosan (CS) solution for 30 min. Next, 10 μL of $Bi_2Sn_2O_7$–NH_2 suspension was dropped onto a fixed area (0.16 cm^2) of ITO surface and dried at room temperature, then the obtained cyclic amplification products (PD) were added to 10 μL of the DNA hydrogel at 37 °C for 1 h for releasing S^{2-} (the processes for cycling amplification and preparation of DNA hydrogel are given in the ESI†). Subsequently, 10 μL of the above solution with S^{2-} was dropped onto the electrode with $Bi_2Sn_2O_7$ and incubated at 37 °C for 10 min, followed by rinsing with double distilled water. Finally, the electrode was dried naturally and the PEC signals were detected for target assay.

Results and discussion

Characterization of the synthesized $Bi_2Sn_2O_7$ samples

X-ray photoelectron spectroscopy (XPS) was used to study the surface chemical state and element composition of the $Bi_2Sn_2O_7$ samples. Fig. 1A shows the full-spectrum scan of XPS for $Bi_2Sn_2O_7$ samples, and it can be seen that Bi, Sn, C and O elements are contained in $Bi_2Sn_2O_7$. Carbon was probably due to the incidental hydrocarbon from the XPS system itself. Fig. 1B shows the Bi 4f XPS spectrum; two strong peaks at 159.4 and 164.7 eV were assigned to Bi $4f_{5/2}$ and Bi $4f_{7/2}$, indicating the presence of Bi^{3+} in the samples. As shown in Fig. 1C, the two peaks of Sn $3d_{5/2}$ and Sn $3d_{3/2}$ were at 486.6 and 495.1 eV due to the existence of Sn^{4+}. In Fig. 1D, the binding energy of element O was 530.3 eV. It is obvious from the strong peak that the sample contains oxygen. The results indicate the successful synthesis of $Bi_2Sn_2O_7$.

Fig. 2A shows the X-ray diffraction (XRD) pattern for $Bi_2Sn_2O_7$ samples. It can be seen that $Bi_2Sn_2O_7$ displays high purity and belongs to the cubic crystalline phase, indicating the successful preparation of $Bi_2Sn_2O_7$. It corresponds to the Joint Committee on Powder Diffraction Standards (JCPDS)

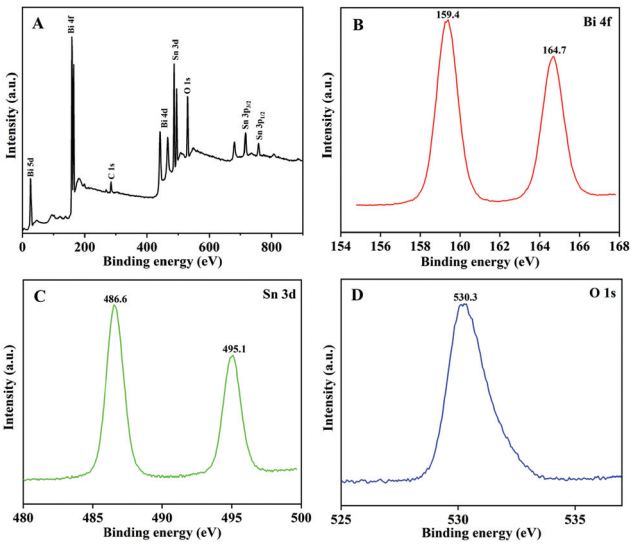

Fig. 1 XPS spectra by full-scan (A) and the corresponding Bi 4f (B), Sn 3d (C) and O 1s (D) of $Bi_2Sn_2O_7$ samples.

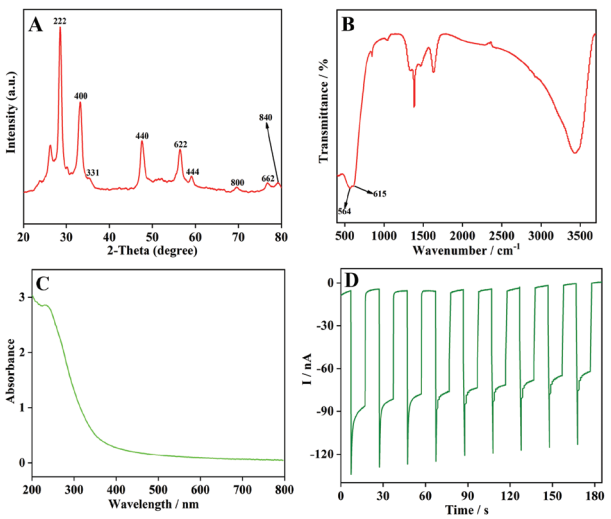

Fig. 2 XRD pattern (A); FT-IR spectrum (B); UV-vis spectrum (C); photocurrent responses (D) of $Bi_2Sn_2O_7$ samples.

card number: 89-5625, and the characteristic peaks are marked in Fig. 2A.[31]

The Fourier transform infrared (FT-IR) spectrum of $Bi_2Sn_2O_7$ is shown in Fig. 2B, and the peaks at about 564 cm^{-1} and 615 cm^{-1} represent the stretching vibration of the Bi–O and Sn–O bond.[30] Fig. 2C shows the UV-vis absorption spectrum of $Bi_2Sn_2O_7$, and the light absorption range was only limited to the ultraviolet region, suggesting that its absorption efficiency for solar energy was low. Fig. 2D shows that the photocurrent signal of $Bi_2Sn_2O_7$ was about −0.13 μA, and it was relatively stable for ten cycles (under 460 nm light irradiation), but the low signal further proved its low utilization for solar energy.

Characterization of the anion exchange reaction

To determine the composition of the product after adding S^{2-} to $Bi_2Sn_2O_7$, XPS was used to analyze pure $Bi_2Sn_2O_7$, Bi_2S_3 and the mixture of $Bi_2Sn_2O_7$ with S^{2-} (Fig. 3A). It was obvious that the mixture contained characteristic peaks of both $Bi_2Sn_2O_7$ and Bi_2S_3, indicating that $Bi_2Sn_2O_7$ and S^{2-} had an anion exchange reaction to form heterojunction $Bi_2Sn_2O_7/Bi_2S_3$. The characteristic peak of S^{2-} in the heterojunction is shown in Fig. 3B. The binding energy of S^{2-} was 225.48 eV, which is consistent with previous reports.[32]

The elemental analysis of $Bi_2Sn_2O_7$ and $Bi_2Sn_2O_7/Bi_2S_3$ was conducted using energy-dispersive X-ray microanalysis (EDS). As shown in Fig. 3C, the $Bi_2Sn_2O_7$ sample mainly contained Bi, Sn, O, Pt, C and Si elements because the $Bi_2Sn_2O_7$ sample was prepared in silicon wafer and it was coated with Pt to increase the conductivity; the C element present in the sample was mainly due to carbon dioxide (CO_2) in the air. The elemental analysis of $Bi_2Sn_2O_7/Bi_2S_3$ is shown in Fig. 3D. Compared to $Bi_2Sn_2O_7$, it also contained S element, indicating that $Bi_2Sn_2O_7$ had an anion exchange reaction with S^{2-}.

Scanning electron microscopy (SEM) images were used to verify the morphology change of $Bi_2Sn_2O_7$ after the anion exchange reaction. As shown in Fig. 4A and B, the morphology of pure $Bi_2Sn_2O_7$ was a porous petal shape with a radius of about 5 μm. The obtained $Bi_2Sn_2O_7/Bi_2S_3$ heterojunction after the anion exchange reaction is shown in Fig. 4C and D. The holes of $Bi_2Sn_2O_7$ were blocked with the generated Bi_2S_3, indicating the success of the anion exchange reaction.

The pure $Bi_2Sn_2O_7$, Bi_2S_3 and the ion exchange product $Bi_2S_3/Bi_2Sn_2O_7$ were further characterized by UV-vis diffuse

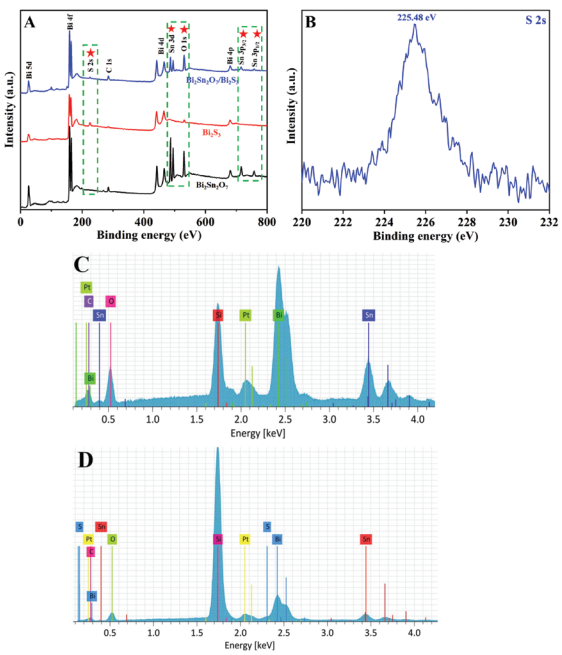

Fig. 3 XPS spectra of $Bi_2Sn_2O_7$, Bi_2S_3 and $Bi_2Sn_2O_7/Bi_2S_3$ (A) and the corresponding S 2s of $Bi_2Sn_2O_7/Bi_2S_3$ (B); EDS of the $Bi_2Sn_2O_7$ (C) and $Bi_2Sn_2O_7/Bi_2S_3$ (D).

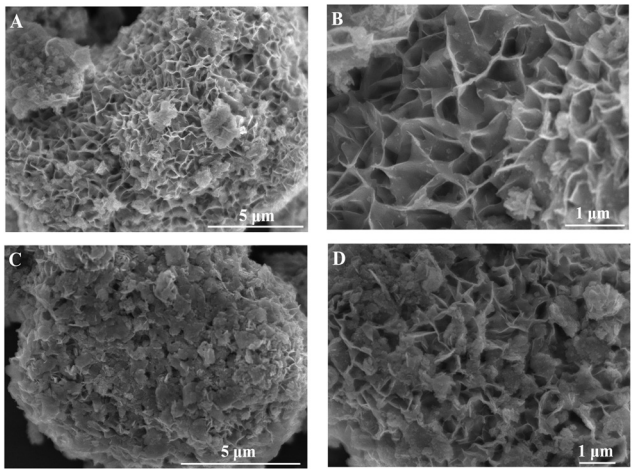

Fig. 4 SEM images of $Bi_2Sn_2O_7$ (A) and (B); SEM images of Bi_2S_3/$Bi_2Sn_2O_7$ (C) and (D).

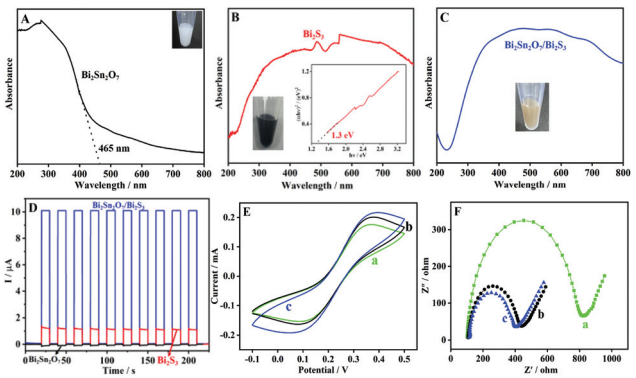

Fig. 5 UV-vis diffuse reflectance spectra of (A) $Bi_2Sn_2O_7$, (B) Bi_2S_3 (inset: Tauc plots of Bi_2S_3) and (C) $Bi_2Sn_2O_7$/Bi_2S_3. (D) Photocurrent responses of $Bi_2Sn_2O_7$ (black curve), Bi_2S_3 (red curve) and $Bi_2Sn_2O_7$/Bi_2S_3 (blue curve). (E) CV and (F) EIS of (a) ITO, (b) ITO/$Bi_2Sn_2O_7$, and (c) ITO/$Bi_2Sn_2O_7$/Bi_2S_3 in 0.1 M PBS containing 5 mM $[Fe(CN)_6]^{3-/4-}$.

reflectance spectra. As shown in Fig. 5A, the $Bi_2Sn_2O_7$ mainly absorbed light below 465 nm, indicating that the energy gap of $Bi_2Sn_2O_7$ was probably 2.67 eV. The absorption range of Bi_2S_3 was the whole UV-vis region (200–800 nm, Fig. 5B). Bi_2S_3 was the indirect-gap semiconductor; its bandgap (E_g) was about 1.30 eV by Tauc equation (ESI†). The E_{VB} and E_{CB} of $Bi_2Sn_2O_7$ were 3.08 eV and 0.41 eV, respectively. As for Bi_2S_3, E_{VB} = 1.42 eV, and E_{CB} = −0.12 eV. Fig. 5C showed that the absorption frequency of the Bi_2S_3/$Bi_2Sn_2O_7$ heterojunction extended to 800 nm, which was similar to that of pure Bi_2S_3. The different colors of the substances also provide evidence about their compositions. As shown in Fig. 5, the colors of pure $Bi_2Sn_2O_7$ and Bi_2S_3 were milk-white and black, while the formed Bi_2S_3/$Bi_2Sn_2O_7$ showed a light brown color. The above characterizations proved that the anion exchange reaction between $Bi_2Sn_2O_7$ and S^{2-} was successful.

The PEC signals of $Bi_2Sn_2O_7$, Bi_2S_3 and the heterojunction Bi_2S_3/$Bi_2Sn_2O_7$ were investigated (Fig. 5D). The signals of the pure $Bi_2Sn_2O_7$ and Bi_2S_3 were −0.13 μA and 1.16 μA, respectively. The signal of the Bi_2S_3/$Bi_2Sn_2O_7$ heterojunction reached 10 μA, which was 76.9 times that of $Bi_2Sn_2O_7$, and 8.6 times that of Bi_2S_3. The comparison of the PEC signals proved that the heterojunction displayed a great PEC sensitization effect. The results also indicated that the light absorption range of the heterojunction Bi_2S_3/$Bi_2Sn_2O_7$ was enlarged and the photogenerated carriers were separated more effectively. Moreover, the photocurrent was converted from the cathode to the anode after forming the heterojunction, thus eliminating the interference of the background signal.

Cyclic voltammetry (CV) and electrochemical impedance spectroscopy (EIS) were used to characterize the anion exchange reaction (Fig. 5E and F). Compared with the bare ITO electrode (curve a), the ITO/$Bi_2Sn_2O_7$ showed increased electrochemical current and decreased EIS value due to the good electrical conductivity of $Bi_2Sn_2O_7$ (curve b). After Bi_2S_3/$Bi_2Sn_2O_7$ was formed *via* the anion exchange reaction, the CV response was further enhanced and EIS decreased (curve c), which indicated that the compound had better electrical conductivity. These electrochemical methods demonstrated that the ion exchange reaction was successful.

Scanning electron microscopy (SEM) image of DNA-hydrogels

Fig. 6A shows the SEM image of the freeze-dried DNA-hydrogels. A highly cross-linked gelatinous structure was observed, indicating that the DNA-hydrogels were successfully prepared.

Characterization of SiO_2-DNA

Fig. 6B shows the SEM image of SiO_2 microspheres. The SiO_2 microspheres were about 300 nm and the size was uniform. Fig. 6C shows the UV-vis absorption spectra of the SiO_2 microspheres (a), DNA (b), and SiO_2-DNA (c). After DNA was attached to the SiO_2 microspheres, the UV absorption peak of DNA appeared at 260 nm (line c), suggesting that the amino-modified DNA was successfully connected to the carboxyl-modified SiO_2 microsphere.

Possible PEC mechanism of the biosensor

The possible PEC mechanism of $Bi_2Sn_2O_7$ was studied (Scheme 2A). Under the irradiation of light, the photo-excited electrons were transferred from the valence band (VB) to the

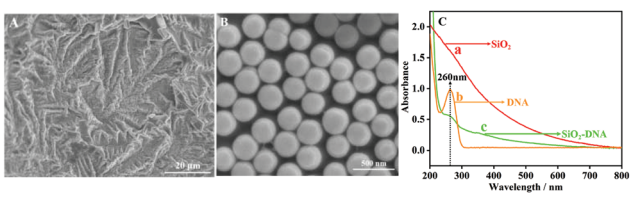

Fig. 6 (A) SEM image of the freeze-dried DNA-hydrogel; (B) SEM image of SiO_2 microspheres; (C) UV-vis absorption spectra of (a) SiO_2 microspheres, (b) DNA, (c) SiO_2-DNA.

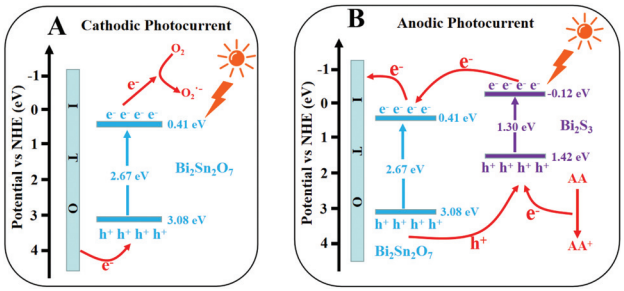

Scheme 2 Schematic diagrams for the PEC processes of $Bi_2Sn_2O_7$ (A) and the $Bi_2Sn_2O_7/Bi_2S_3$ heterojunction (B).

conduction band (CB), leaving holes in the valence band. Then, electrons in the conduction band continually reduced dissolved oxygen in solution to oxygen radical anions, and electrons were supplied from the electrode to the valence band due to electrostatic attraction, producing a cathodic photocurrent.

When the hydrogel-released S^{2-} had an anion exchange reaction with $Bi_2Sn_2O_7$, the heterojunction $Bi_2Sn_2O_7/Bi_2S_3$ was obtained. The values of the CB, VB and E_g of the two materials were calculated (Fig. 5), which were consistent with the traditional type II heterojunction.[33] The corresponding charge transfer process is shown in Scheme 2B. Under the excitation of light, the electrons of the two materials were transferred from the VB to CB, leaving holes in the VB. It was clear that the CB and VB levels of Bi_2S_3 were higher than those of $Bi_2Sn_2O_7$, so the electrons in Bi_2S_3 were transferred to $Bi_2Sn_2O_7$, and the holes in $Bi_2Sn_2O_7$ were transferred to Bi_2S_3. As an electron donor, AA consumed the photogenerated holes in the VB of the heterojunction, which reduced the recombination rate of the electron–hole pairs. Thus, the photogenerated carriers were effectively separated and resulted in a very high anodic photocurrent accompanied by polarity conversion.

Polyacrylamide gel electrophoresis (PAGE) characterization of target recycling amplification and DNA-hydrogel

The target recycling amplification process was characterized by PAGE. In Fig. 7A, lane M is the marker, lane 1, lane 2 and lane 3 were capture DNA (CP), product chain (PD) and target DNA, respectively. Lane 4 displayed the hybridization result of CP and PD; the band at the higher position suggests that the two DNA chains were successfully hybridized.

When target DNA was further added, the band in lane 5 migrated more slowly, indicating that the hybridization of CP with PD and the target was successful. After adding Exo III, the product (CP + PD + target) was hydrolyzed to the target and product PD (lane 6), suggesting the target-induced amplification process was achieved.

Fig. 7B verified the formation process of the DNA-hydrogels. Lane M to lane 4 are the marker, ssDNA P1, ssDNA P2, linker DNA (LK), product DNA PD in sequence. When the molecular weight is larger, DNA runs slower, so the top band in lane 5 suggests the successful hybridization of P1, P2 and LK. When the product chain PD was added, PD hybridized with LK to replace P1 and P2 (lane 6), and a band appeared at the highest location, which proved that target PD can open the DNA-hydrogel to release S^{2-} for PEC biosensing.

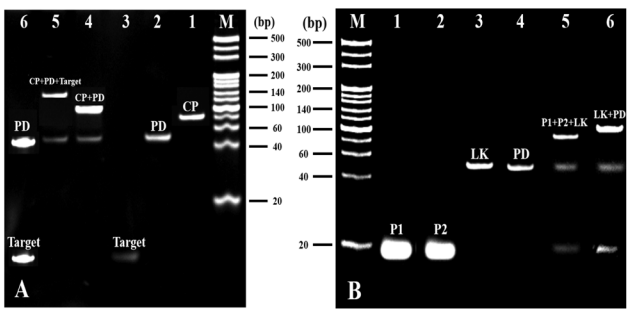

Fig. 7 PAGE analysis of Exo III-assisted target recycling amplification (A), the formation of DNA-hydrogel (B).

Optimization of experimental conditions

The concentration of photoactive nanomaterials directly affected the photoelectric signal. If the concentration was too low, fewer photogenerated electrons and hole pairs would generate a lower PEC signal. In contrast, a too high concentration can result in the low transmittance of light and thus, a low PEC signal, so the concentration of $Bi_2Sn_2O_7$ was optimized (Fig. S1A†). With the increasing concentration of $Bi_2Sn_2O_7$, the PEC signal firstly increased then decreased, and the maximum value was 0.5 mg mL^{-1}, indicating that the best concentration was 0.5 mg mL^{-1}.

The effect of ascorbic acid (AA) concentration on the PEC signal was also studied. Ascorbic acid has strong reducibility, which can provide electrons to neutralize holes in photoactive materials, thus accelerating the efficient transfer of photogenerated charges and enhancing the photocurrent signal. However, too much ascorbic acid may affect the pH of PBS and thus the photocurrent signal decreased, so the best dosage was 0.1 M (Fig. S1B†).

The dosage and incubation time of the Exo III enzyme are important for target cycle amplification in the sensing system, so they were also investigated. The photoelectrochemical signal was enhanced with increasing amounts of Exo III, and no obvious change was observed after 10 U of Exo III (Fig. S1C†). Therefore, 10 U of Exo III was used for detection. Fig. S1D† shows that the PEC signal was enhanced with the prolongation of incubation time for Exo III. When the time exceeded 2 hours, the PEC signal tended to be flat and no longer increased; hence, 2 hours was selected as the optimized incubation time for Exo III in the detection system.

According to the previous report,[14] deoxygenation was very important for the formation of the DNA hydrogel, so the deoxygenation time was optimized. Fig. S2A† shows that the signal gradually increased with increasing deoxygenation time until 15 min, then there was almost no signal change, indicating that the optimized deoxygenation time for forming DNA hydrogel was 15 min.

To study the destruction of the DNA hydrogel for releasing S^{2-} in the biosensing process, the hybridization of the DNA chain PD and LK was very critical for the process. Therefore, the incubation time and temperature of hybridization were optimized. From Fig. S2(B) and Fig. S2(C),† the optimal reaction temperature was 37 °C and the optimal incubation time was 60 min.

The concentration of S^{2-} directly affected the ion exchange reaction, and then affected the photoelectric signal and sensitization efficiency; therefore, the concentration of S^{2-} was optimized. From Fig. S2(D),† the photoelectrochemical signal increased continuously until 50 mM, then decreased with the increasing concentration of Na_2S, which may be caused by the proportion of $Bi_2Sn_2O_7$ and Bi_2S_3 in the compound; therefore, the sensitization efficiency was the best with 50 mM Na_2S.

The amount of acrylamide had an effect on the DNA hydrogel; when the amount of acrylamide was high, the viscosity of the formed gel was high, and the sulfur ions were coated more firmly. However, the light transmittance of the photoelectric material decreased with the increased viscosity, so the amount of acrylamide was optimized. When the acrylamide dosage was 3%, the PEC signal reached a peak of 8.2 μA (Fig. S3A†), and enough S^{2-} was coated in the DNA hydrogel, so 3% was used for the DNA hydrogel.

Silicon dioxide microspheres were used for binding the capture chain (CP) *via* covalent bonds, the concentration and activation time of EDC and NHS were optimized. When the concentrations of EDC and NHS were 5 mg mL^{-1} and the activation time was 1.5 h, the highest PEC signal was achieved (Fig. S3B and S3C†).

The time of the ion exchange reaction was also optimized (Fig. S3D†). The reaction was very fast and took only 10 minutes, which also displayed the advantage of the PEC biosensor.

The detection performance of the biosensor

Under optimal reaction conditions, the feasibility of the PEC biosensor was investigated. Fig. 8A (inset) displays the PEC signals of $Bi_2Sn_2O_7$ (curve a) and $Bi_2Sn_2O_7/Bi_2S_3$ by anion-exchange reaction (curve h). In the presence of a 10 nM target, the PEC signal of the biosensor reached 8.2 μA (curve h), suggesting that the PEC sensitization amplitude of $Bi_2Sn_2O_7/Bi_2S_3$ was increased by 63 times. The results indicated that the PEC biosensor can be used for the quantitative detection of target DNA with outstanding sensitivity.

Fig. 8A shows the PEC responses of the biosensor to different target concentrations from 10 fM to 10 nM, and the PEC current rises with the increase in DNA concentration (curves b to h). The PEC signal changes exhibited a linear relationship to the target concentrations in the range of 100 fM–10 nM (Fig. 8B). The linear regression equation is $y = 20.64 + 1.51 \lg x$ ($R^2 = 0.997$). The results suggest that this PEC biosensor can be applied for sensitive DNA detection. Furthermore, the detection limit was 20 fM, indicating this biosensor is more sensitive than the previously reported methods (Table S2†), and has promising applications in clinical tests.

The selectivity of the PEC biosensor and application for detecting target DNA in human serum samples

The selectivity of the biosensor was verified by using the interference DNA sequences. As shown in Fig. S4,† the PEC response of the target is 2.1 times that of the single-base mismatched target, and 4.3 times that of the two-base mismatched target. However, for the random sequence and non-complementary DNA, there was almost no PEC signal, indicating that the PEC biosensor has high specificity for target detection.

To prove the application of the biosensor in human serum samples, different concentrations of targets were added to the diluted serum and the recoveries were calculated. The results are presented in Table S3,† and the recoveries ranged from 95.8% to 103.5%, indicating that the proposed biosensor has potential for application in real sample assays.

Conclusions

In conclusion, a novel $Bi_2Sn_2O_7/Bi_2S_3$ heterojunction PEC biosensor based on anion exchange coupled with a unique DNA hydrogel was reported for DNA detection. This PEC platform has several advantages. Firstly, a new target-responsive DNA hydrogel was flexibly designed to load S^{2-} for the $Bi_2Sn_2O_7/Bi_2S_3$-based PEC biosenor. Secondly, it was discovered that a tremendous PEC sensitization effect can be achieved simply by an *in situ* anion exchange reaction between S^{2-} and $Bi_2Sn_2O_7$, and the PEC sensitization amplitude was increased by 63 times. Thirdly, this developed PEC biosensor realized the photocurrent polarity switching from cathodic to anodic, removing most of the interference of the background signal. The operation procedure is simple and convenient, and only S^{2-} was released from the DNA hydrogel for PEC biosensing. Considering the above advantages, this work provides a promising heterojunction nanomaterial for the PEC biosensing plat-

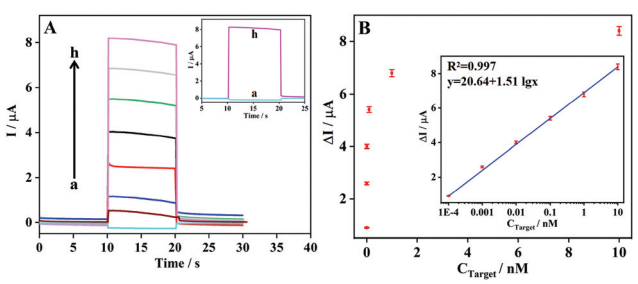

Fig. 8 (A) PEC responses of the biosensor to different target concentrations: 0, 10 fM, 100 fM, 1.0 pM, 10 pM, 100 pM, 1.0 nM and 10 nM (from a to h); the inset shows the PEC responses of the electrode with $Bi_2Sn_2O_7$ (curve a) and $Bi_2Sn_2O_7/Bi_2S_3$ by an ion-exchange reaction from the target-triggered DNA hydrogel (curve h). (B) The relationship of the PEC signal changes to target concentrations; inset is the calibration plot for target detection ($\Delta I = I - I_0$).

form, which can be used for the sensitive detection of various biomarkers.

Conflicts of interest

There are no conflicts to declare.

Acknowledgements

This work was supported by the National Natural Science Foundation of China (No. 22076089).

Notes and references

1 M. Gratzel, *Nature*, 2001, **414**, 338–344.
2 Z. Kang, X. Yan, Y. Wang, Y. Zhao, Z. Bai, Y. Liu, K. Zhao, S. Cao and Y. Zhang, *Nano Res.*, 2015, **9**, 344–352.
3 Y. Zang, J. P. Lei and H. X. Ju, *Biosens. Bioelectron.*, 2017, **96**, 8–16.
4 M. Wang, H. S. Yin, N. N. Shen, Z. N. Xu, B. Sun and S. Y. Ai, *Biosens. Bioelectron.*, 2014, **53**, 232–237.
5 L. Ge, Q. Liu, N. Hao and K. Wang, *J. Phys. Chem.*, 2019, **7**, 7283–7300.
6 N. Hao, Z. Dai, M. Xiong, R. Hua, J. W. Lu and K. Wang, *Sens. Actuators, B*, 2020, **306**, 127594.
7 N. Hao, R. Hua, S. B. Chen, Y. Zhang, Z. Zhou, J. Qian, Q. Liu and K. Wang, *Biosens. Bioelectron.*, 2018, **101**, 14–20.
8 J. Ran, W. Guo, H. Wang, B. Zhu, J. Yu and S. Z. Qiao, *Adv. Mater.*, 2018, **30**, 1800128.
9 S. Chen and L. W. Wang, *Chem. Mater.*, 2012, **24**, 3659–3666.
10 K. Vinodgopal and P. V. Kamat, *Environ. Sci. Technol.*, 1995, **29**, 841.
11 K. Ranjit and B. Viswanathan, *J. Photochem. Photobiol., A*, 1997, **108**, 79.
12 Y. S. Huang, Y. L. Ma, Y. H. Chen, X. M. Wu, L. T. Fang, Z. Zhu and C. J. Yang, *Anal. Chem.*, 2014, **86**, 11434–11439.
13 J. Liu, *Soft Matter*, 2011, **7**, 6757–6767.
14 C. L. Li, H. K. Li, J. J. Ge and G. F. Jie, *Chem. Commun.*, 2019, **55**, 3919.
15 L. Zhang, J. P. Lei, L. Liu, C. F. Li and H. X. Ju, *Anal. Chem.*, 2013, **85**, 11077–11082.
16 Y. S. Huang, Y. L. Ma, Y. H. Chen, X. M. Wu, L. T. Fang, Z. Zhu and C. Y. Yang, *Chem. Commun.*, 2011, **47**, 9312–9314.
17 J. Hur, K. Im, S. W. Kim, U. J. Kim, J. Lee, S. Hwang, J. Song, S. Kim, S. Hwang and N. Park, *J. Mater. Chem. A*, 2013, **1**, 14460–14466.
18 S. P. Liu, W. Q. Su, Y. L. Li, L. L. Zhang and X. T. Ding, *Biosens. Bioelectron.*, 2018, **103**, 1–5.
19 Y. He, X. Yang, R. Yuan and Y. Q. Chai, *Anal. Chem.*, 2017, **89**, 8538–8544.
20 Y. Chen, Q. Wang, J. Xu, Y. Xiang, R. Yuan and Y. Q. Chai, *Chem. Commun.*, 2013, **49**, 2052.
21 J. A. Rasquinha, A. Bej, S. Dutta and S. Mukherjee, *Biochemistry*, 2017, **56**, 4962–4971.
22 A. Petitjean, E. Mathe, S. Kato, C. Ishioka, S. V. Tavtigian, P. Hainaut and M. Olivier, *Hum. Mutat.*, 2007, **28**, 622–629.
23 J. E. Satterwhite, A. M. Pugh, A. S. Danell and E. G. Hvastkovs, *Anal. Chem.*, 2011, **83**, 3327–3335.
24 J. Tan, M. M. Zhao, J. Wang, Z. H. Li, N. Liang, L. Q. Zhang, Q. Yuan and W. H. Tan, *Angew. Chem., Int. Ed.*, 2018, **58**, 1621–1625.
25 Y. Noori and K. Akhbari, *RSC Adv.*, 2017, **7**, 1782–1808.
26 H. Li, R. Brescia, M. Povia, M. Prato, G. Bertoni, L. Manna and I. Moreels, *J. Am. Chem. Soc.*, 2013, **135**, 12270–12278.
27 M. V. Kovalenko, R. D. Schaller, D. Jarzab, M. A. Loi and D. V. Talapin, *J. Am. Chem. Soc.*, 2012, **134**, 2457–2460.
28 Q. A. Akkerman, A. Genovese, C. George, M. Prato, I. Moreels, A. Casu, S. Marras and A. Curcio, *ACS Nano*, 2015, **9**, 521–531.
29 B. Q. Jia, W. Zhao, D. Sun, L. G. Fan, H. L. Yao, P. Lu, F. F. Xu and F. Q. Huang, *Chem. Mater.*, 2019, **31**, 9532–9539.
30 J. T. Cao, B. Wang, Y. X. Dong, Q. Wang, S. W. Ren, Y. M. Liu and W. W. Zhao, *ACS Sens.*, 2018, **3**, 1087–1092.
31 D. Li and J. Q. Xue, *New J. Chem.*, 2015, **39**, 5833.
32 H. K. Li and G. F. Jie, *Analyst*, 2020, **145**, 5524–5531.
33 J. X. Low, J. G. Yu, M. Jaroniec, S. Wageh and A. A. Al-Ghamdi, *Adv. Mater.*, 2017, **29**, 1601694–1601714.